Surface-generated copper ions induce multilayer growth of small peptides

Jessem Landoulsi, Vincent Dupres, Christophe Méthivier, Ivan Leteyi Mfiban, Pauline Cornette, Elodie Colaço, Claire-Marie Pradier

Surface-generated copper ions induce multilayer growth of small peptides

Jessem Landoulsi [a *], *Vincent Dupres* [b], *Christophe Methivier* [a], *Ivan Leteyi Mfiban* [a], *Pauline Cornette* [a], *Elodie Colaço* [a], *Claire-Marie Pradier* [a, *]

[a] Sorbonne Université, CNRS, Laboratoire de Réactivité de Surface, 4 place Jussieu, F-75005, Paris, France.

[b] Cellular Microbiology and Physics of Infections – Lille Center for Infection and Immunity, Institut Pasteur de Lille, CNRS, INSERM, University of Lille, Lille, France

Corresponding Authors

* C.M. Pradier (claire-marie.pradier@sorbonne-universite.fr)

* J. Landoulsi (jessem.landoulsi@sorbonne-universite.fr)

Abstract

Herein, we investigate the adsorption behavior of a small peptide, Glu-Cys-Gly, in aqueous solution onto copper surface and unravel a mechanism of growth of a hybrid peptide-copper multilayer the thickness of which may exceed a hundred of nanometers. Thanks to a combined set of surface characterizations supported by theoretical considerations, we provide a comprehensive understanding of the driving force and parameters influencing multilayer growth. (i) The generation of Cu^+ ions due to the dissolution of copper surface, modulated by pH, results in the formation of cuprous-thiolate complex made of two peptide molecules anchoring one Cu^+ cation. (ii) The stability of this hybrid multilayers is ensured by intermolecular interactions between peptide-copper entities mainly through a combination of electrostatic interaction and hydrogen bonds which stabilize the supramolecular edifice.

Keywords: Oligopeptide; adsorption; XPS; AFM; hybrid layer.

1. Introduction

Exploring the interfaces between biomolecules and inorganic materials is a widely explored topic for its fundamental relevancy and strategic implication in many fields, such as biomaterials science and nanotechnologies. [1, 2] This is closely related to the high versatility of biological molecules and their aptitude to be involved in unique specific interactions both with soft and hard matter. Peptides usually bind to inorganics in very specific ways and this has been exploited in various applications such as self-assembly for surface biocompatibility, crystal growth regulation or molecular electronics. [3-6]

Small peptides are oligopeptides made of only few amino acids. Their self-assembly in solution has been the subject of a vast literature, because of their outstanding ability to organize and form a rich repertoire of various nanostructures. [7] By contrast, little work has been devoted to their self-assembly on inorganic solids, and more generally to their adsorption on solid surfaces in aqueous solutions. Yet, some papers have reported promising results regarding their use in biosensing, [8-10] biomineralization [11, 12] or for the control of cell-material interaction. [13]

Thanks to their "simpler" molecular structure, compared to biomacromolecules, small peptides are relevant candidates to progress towards the understanding of complex bio-interfaces.[14] Interestingly, these interfaces can be investigated following a surface science approach, and getting information at the (supra)molecular level.[15-17] This of course calls for modelling in complement to experiments under controlled conditions, namely in UHV. [14, 18] Studies, either theoretical or experimental, dealing with the adsorption of short peptides in aqueous solutions of biological interest are, however, scarce. [19] Moreover, experiments are mostly conducted on inorganic surface with low reactivity in the studied medium, typically Au, SiO_2, YiO2, and TiO_2, widely investigated [20-22], to exclusively focus on the adsorption behaviour of the peptide, while

considering that the surface remains almost chemically inert. The situation is more complex for materials highly reactive in aqueous solutions; this is, obviously the case of a copper surface. [23] Accordingly, understanding the multiple interfacial processes requires characterizing the adsorbed phase in the aqueous medium and monitoring real-time events with the aim to decipher possible evolutions at each side of the interface: metal/oxide surface and the biomolecule of interest.

In the present article, we report a thorough investigation of a tri-peptide/copper interface, with a special attention to the growth mechanism of multilayers and parameters influencing this process. The Glu-Cys-Gly sequence, commonly called L-glutathione (see molecular structure in Figure 1A), was adsorbed onto a copper surface in aqueous solution. This peptide has been used as a physiologically relevant model molecule to investigate its interaction with inorganic nanoparticles. [24] Moreover, it is highly involved in redox processes in eukaryotic cells, particularly in the defense of cells against oxidative stress ; [25, 26] it is oxidized to glutathione disulfide, then regenerated enzymatically or transported via specific proteins in the extracellular space. Here, the adsorption behavior of Glu-Cys-Gly peptide onto copper surface is monitored *in situ* by means of quartz crystal microbalance with dissipation monitoring (QCM-D), both mass and dissipation evolutions bringing information of great interest. The peptide layer is also characterized in the hydrated phase by means of atomic force spectroscopy (AFM) and in the dried sate using X-ray photoelectron spectroscopy (XPS) and polarization modulation- infrared reflexion absorption spectroscopy (PM-IRRAS).

2. Experimental section

2.1. Materials and solutions

Polycrystalline copper wafers specimens of 1×1 mm^2 cut from a ~2 mm thick plate, Cu 99.5 %, from GoodFellow, France) were used in this study. The samples were mechanically polished with

SiC papers of 600; 1200 and 4000 grain size (both sides) followed by fine polishing with 3, and 1 mm diamond suspensions (Struers, France). The samples were then rinsed and sonicated (Branson, USA) in a mixture (50/50%, v/v) of ultrapure water (MilliQ, Millipore, France) and ethanol (HPLC grade, ≥99%, Sigma-Aldrich, France), thoroughly rinsed with ultrapure water and dried under nitrogen gas flow. The samples were used for adsorption tests immediately after surface preparation.

2.2. Adsorption procedure

Glu-Cys-Gly peptide from Sigma-Aldrich (France) was used in this study. Its molecular structures are given in Figure 1A. Peptide solutions were prepared in ultrapure water at concentrations ranging from 0.1 to 10 mM. The pH was adjusted at 3 or 7 (± 0.2) by addition of HCl or NaOH (0.1 M), and the final mixture was vortexed then immediately used for adsorption tests. Copper samples were placed in glass Petri dishes containing the peptide solution and incubated under gentle stirring. After the desired period of adsorption is reached, the samples were rinsed in three different baths (2 min each) of ultrapure water.

2.3. Quartz crystal microbalance with dissipation monitoring (QCM-D)

The adsorption of peptides on the copper substrate was monitored in situ by QCM-D. Measurements were performed using a Q-Sense E1 System (Biolin Scientific, Västra Frölunda, Sweden) at a temperature of 22.0 ± 0.1°C. QCM-D sensors with a reactively sputter-coated film of copper (QSX313) were provided by Q-Sense. They were cleaned by UV/ozone treatment for 15 min prior to use. Oscillations of the crystal at the resonant frequency (5 MHz) or at one of its overtones (15, 25, 35, 45, 55, 65 MHz) were obtained when applying ac voltage. The variations of the resonance frequency (Δf) and of dissipation (ΔD) were monitored upon adsorption of peptides. Solutions were injected into the measurement cell using a peristaltic pump (Ismatec IPC-N 4) at a

low flow rate (30 µL/min). Prior to peptide adsorption, ultrapure water was injected up to signal stabilization, characterized by a low and uniform frequency shift due to weak dissolution of copper. The peptide solution was then brought into the measurement cell for about 40 min. Subsequently, rinsing was performed using ultrapure water until the frequency and dissipation signal reached a stationary value.

For homogenous and rigid adsorbed layer, the frequency changes of the crystal recorded at the resonant frequency superimpose with the signals recorded for the harmonics. In this case, frequency shifts is proportional to the mass of the adsorbed compounds, and can be described using the Sauerbrey equation:

$$\Delta f = -N \times (\Delta m / C_f)$$

where C_f is the mass sensitivity constant and $N = 1, 3, 5, \ldots$ is the number of overtones.

2.4. Atomic force microscopy (AFM)

AFM images were recorded using a commercial AFM (NanoScope VIII MultiMode AFM, Bruker Nano Inc- Nano Surfaces Division, Santa Barbara, CA.) equipped with a 150 × 150 × 5 µm scanner (J-scanner). A quartz fluid cell was used to this end. Copper samples were fixed on a steel sample puck using adhesive tape. The mounted samples were immediately transferred into the AFM liquid cell taking care to avoid dewetting. Images were recorded in peak force tapping mode in ultrapure water at room temperature (~22°C) using oxide-sharpened microfabricated Si_3N_4 cantilevers (Bruker Nano Inc- Nano Surfaces Division, Santa Barbara, CA.). The spring constants of the cantilevers were ranging from 0.2 to 0.5 N/m as determined by the thermal noise method. The curvature radius of silicon nitride tips was lower than 10 nm (manufacturer specifications). Different cantilevers were used for imaging and scratching tests. All images shown in this paper are flattened raw data.

2.5. Polarization modulation – infrared reflexion absorption spectroscopy (PM-IRRAS)

Spectra were recorded on a commercial Thermo scientific (France) Nexus spectrometer. The external beam was focused on the sample with a mirror, at an optimal incident angle of 80°. A ZnSe grid polarizer and a ZnSe photoelastic modulator, modulating the incident beam between p- and s-polarizations (HINDS Instruments, PEM 90, modulation frequency = 37 kHz), were placed prior to the sample. The light reflected at the sample was then focused onto a nitrogen-cooled MCT detector. All presented spectra were obtained from the sum of 128 scans recorded with a 8 cm^{-1} resolution.

2.6. X-ray photoelectron spectroscopy (XPS)

XPS analyses were performed using a ESCA+ spectrometer (Omicron NanoTechnology), equipped with a monochromatized aluminum X-ray source (powered at 20 mA and 14 kV) and a MCD 128 channeltrons detector. Charge stabilization was insured using the CN10 device with an emission current of 5.0 µA and a beam energy of 1 eV. Analyses were performed in the sweeping mode; the resulting analyzed area was 1 mm in diameter. A pass energy of 20 eV was used for narrow scans. Under these conditions, the full width at half maximum (FWHM) of the Ag 3d5/2 peak of a clean silver reference sample was about 0.6 eV. The pressure in the analysis chamber was around 10^{-10} torr. Unless it is specified elsewhere, the photoelectron collection angle, θ, between the normal to the sample surface and the analyzer axis was 45°.The following sequence of spectra was recorded: survey spectrum, C 1s, O 1s, N 1s, Cu 2p, Cu LMN, S 2p and C 1s again to check for charge stability as a function of time and the absence of sample degradation. The binding energy scale was set by fixing the C 1s component due to carbon only bound to carbon and hydrogen at 284.8 eV. The data treatment was performed with the CasaXPS software (Casa Software Ltd., UK). The peaks were decomposed using a linear baseline, and a component shape

defined by the product of a Gaussian and a Lorentzian function, in the 70:30 ratio, respectively. Molar fractions were calculated using peak areas normalized on the basis of acquisition parameters and sensitivity factors provided by the manufacturer. Two independent sets of samples were analyzed by XPS to check the reproducibility.

2.7. Computational methods

Previous to Ab Initio Molecular Dynamic (AIMD) simulations, we optimized molecules using the periodic density functional theory (DFT) method based on the generalized gradient approximation (GGA), [27] employing the Perdew, Burke and Ernzerhof (PBE) [28] exchange-correlation functional as implemented in the plane-wave program Vienna ab initio simulation package (VASP). [28] The projector-augmented wave (PAW) potentials [29, 30] were used for the core electron representation with a PAW core radius of 1.52 Å for oxygen. In this work, the energy cutoff (Ecut) in use was 400 eV. Dispersion forces were considered in the D2 Grimme approach. [31] When the forces were inferior to 10^{-6} eV per cell, the geometry optimizations performed were considered converged.

DFT-based AIMD simulations within the framework of the Born−Oppenheimer approximation have been performed with the CP2K/Quickstep package based on a hybrid Gaussian and plane wave method. [32] The PBE exchange-correlation density functional was used. For all elements, Goedecker−Teter−Hutter pseudopotential [33]and a double-ζ (DZVP) plus polarization Gaussian basis set for the orbitals were used. An energy cutoff of 400 Ry is used. The Grimme D2 method was used in order to take into account VdW forces. Only the gamma point was considered. AIMD simulations were conducted in the microcanonical ⟨NVE⟩ ensemble at 300K with a timestep of 0.5 fs.

3. Results and discussion

The adsorption of Glu-Cys-Gly peptide on the copper surface was monitored *in situ* using QCM-D. Results showed a strong shift in resonance frequency, Δf, around -200 Hz after about 2 min of peptide adsorption (Figure 1B). Δf continued, then, to progress towards negative values and leveled-off after a subsequent rinsing to reach values near -800 Hz after about 40 min of adsorption. In contrast, the dissipation, ΔD, only slightly increased, after injection of the peptide solution, to reach a value of 1.2×10^{-6} at saturation; it turned then close to its initial value (ΔD ~0.2×10^{-6}). The reversible evolution of the dissipation signal is typical of a change in the solution viscosity (water vs peptide aqueous solution). Combined together, Δf and ΔD evolutions suggest the formation of a rigid film. This is consistent with the fact that frequency shifts recorded at the resonant frequency superimpose with those recorded for the harmonics (data not shown). More importantly, the tremendously high Δf values, uncommon for small molecules, are indicative of an extensive adsorption of the peptide on the copper surface. Δf noticeably exceeds the values obtained with common globular proteins (~30-60 kDa); [34-37] it is comparable to frequency shifts observed with fibrillar protein layer (~ 300 kDa). [38, 39] Also, the very low dissipation value, suggests the formation of a peptide layer with a low hydration rate.

The following experiment was performed in order to assess the possible role of copper itself in the formation of such a thick and poorly hydrated layer. For this purpose, Glu-Cys-Gly peptide adsorption was performed on gold surface ; from previous investigations,[40-42] the formation of a monolayer of peptide was reported. In the present study, the peptide adsorption on gold led, indeed, to only slight frequency shift, -8 Hz at a maximum and -4.5 Hz after subsequent rinsing (Figure 1C). By using Sauerbrey relationship, the adsorbed mass, which acts as a rigid adlayer, could be evaluated, yielding a molecular density of about 1.5 molecule/nm^2, which is comparable to previous findings. [41]

The Glu-Cys-Gly layer, formed on copper, was further characterized by AFM imaging in the liquid phase (under rinsing conditions). AFM images recorded prior to and after the adsorption of the peptide are presented in Figures 2A and B. The bare copper surface (before peptide adsorption) was quite smooth surface (R_{rms} = 1.8 nm, Figure 2A). After adsorption of peptides (10 mM, 1 h), the roughness strikingly increased (R_{rms} = 5.8 nm), the film being constituted of fairly regular packing of particles (Figure 2B). The height of these particle aggregates was ranging from about 2 to 10 nm, the real particle height being difficult to evaluate reliably because the tip was too large to penetrate into the interstices between particles (see cross-section, Figure 2B). In order to estimate the thickness of the peptide layer, a 2 µm × 2 µm area was scratched by the AFM tip at a high applied force, and the layer thickness was measured using the cross-section as shown in Figure 2C; this was done in the presence of solvent (hydrated state of the film). It is worth noting that when this procedure was applied to the bare copper surface, i.e. before peptide adsorption, no discernable scratched zone was observed due to the stiffness of the substrate (not shown). The average thickness of peptide layer obtained after 1 h adsorption at 10 mM was about 50 nm, thus confirming the formation of a thick layer. Moreover, the thickness strongly increased with increasing the peptide concentration in solution going to values near 100 nm at 100 mM (Figure 2D).

The chemical composition of the peptide layer was probed by XPS analyses in the dried state, i.e. after peptide adsorption, subsequent rinsing and drying. Typical C 1s, N 1s and S 2p peaks recorded on the peptide adlayer are given in (Figure S1, SI). Special attention is dedicated to the sulfur and copper signals which provide relevant information regarding the copper/peptide interface (Figure 3A). The S 2p peak was decomposed into a well-defined single doublet, the distance between the S $2p_{3/2}$ and S $2p_{1/2}$ components being set at 1.18 eV, and a ratio of 2 was

imposed between their respective intensities. The binding energy position of S $2p_{3/2}$ component, ca. 162.4 eV, can be assigned to bound thiolate, and no unbound thiols or oxidized sulfur species, with expected contributions at ca. 163-164 and 168 eV, respectively, could be identified, regardless of the concentration of peptide solution.

As for the Cu $2p_{3/2}$, after immersion at low concentration, 0.1 mM (and rinsing), two contributions could be identified, one at ~932.3 eV due to Cu^0 and/or Cu^I compounds and one at ~935 eV, together with a slight and broad "satellite" peak at higher binding energies, attributed to Cu^{II} components (Figure 3A). After immersion at higher concentration, 0.1 or 10 mM, the contributions attributed to Cu^{II} completely disappeared.

The precise attribution of the 932.3 eV contribution was made by considering the so-called "modified Auger parameter", α'.[1] Typical $CuL_3M_{45}M_{45}$ Auger spectra recorded on copper surface prior to and after the adsorption of peptides at 10 mM are presented in Figure S2 (SI). The calculated values of α'_{Cu}, given in Table S1 (SI), suggest that the adlayer is wholly composed of Cu^I-containing compounds.

Besides, angle-resolved XPS (AR-XPS) measurements (see Figure 3B), did not show changes in the S 2p peak profile when passing from 5 to 80° take-off angle (Figure 3A). In other words, sulfur is mainly involved in copper-thiolate bonds throughout the whole layer. Moreover, the S/Cu molar concentration ratio, passes from 1 to 2 for peptide concentrations equal to 0.1 and 1, or 10 mM, respectively (Figure 3C). This strongly suggests the formation of Cu^I-peptide complexes on the surface with a peptide over Cu^I ratio close to 1:2. Note that the S/Cu ratio is close to 1 at low

[1] $\alpha' = E_K(C'C''C''') + E_B(C)$, where $E_K(C'C''C''')$ is the kinetic energy of an Auger transition involving C', C'', and C''' core electron levels; α'_{Cu}, was calculated by using the Cu $2p_{3/2}$ and Cu LMM peaks.

peptide concentration (0.1 mM), likely due to the low thickness (<10 nm) of the peptide adlayer which allows a contribution of Cu signal from the underlying copper substrate to be detected.

The synthesis of bulk copper (I)-thiolate complexes has been, indeed, reported in the literature because of their significant interest to unravel the behavior of cysteine-rich copper metalloproteins. [43, 44] Particularly, various compounds have been obtained at different S:Cu ratios, including 2:1 ratio, but the synthesis procedures were restricted to organic solvents. [45-47] Besides, in solid state, it has been reported that Cu^+ ions and alkanethiols may form multilayered copper (I)-thiolate complexes. [48] On solid surfaces, the mechanism by which thiol-containing molecules interact with copper substrates has been the subject of a vast literature over the past two decades,[49-57] and has still attracted a growing interest. [58-64] Experiments have been mostly performed with alkanethiols in ethanol and, more recently, through vapor-phase deposition.[59, 60, 63] All these studies have led to the conclusion that the adsorption process involves the reduction of the native oxide layer, present on the metal surface, and the oxidation of thiols (RS–H) to disulfides (RS–SR), as observed by gas chromatography-mass spectrometry experiments.[52] The self-assembly of thiols occurs, thus, on the reduced copper surface, yielding a cuprous-thiolate complex ($RS–Cu^I$). While alkanethiols mostly form self-assembled monolayers on gold surfaces, they may grow on copper substrate into multilayers the properties of which has been well described in recent papers. [59, 62] In aqueous solutions, studies have essentially reported the adsorption of cysteine on copper surface. [65-67] Liedberg et al. have suggested that the formation of cysteine multilayers is due to the presence Cu^+ cations within the layer. [68] In the present study, the involvement of Cu^+ ions in the adsorption of Glu-Cys-Gly peptide and the resulting thick layer is examined by considering the rate of copper dissolution, in water, at different pH values, measured by QCM-D. At pH 7, a weak and uniform positive frequency shift was observed due to a slow dissolution of

copper surface, while at pH 3 this process was strongly accelerated (Figure S3A, SI). The gradient, d(Δf)/dt, determined at pH 7 and 3 increased from about 2.5 to about 20 Hz.min^{-1} (Figure S3B, SI), indicating an enhancement of copper dissolution at acidic pH, in agreement with previous observations, [69] and thermodynamic predictions.

Adsorption of the Glu-Cys-Gly peptide, was then monitored by PM-IRRAS after immersion in peptide solution (10 mM) at pH 3 or 7 (see Figure 4). Bands characteristic of the peptide molecule were observed (Figure 4A and B): amide I and II bands at 1650 and 1554 cm^{-1}, a vibration band associated to the symmetric stretching modes of the $-COO^-$ moiety at about 1412 cm^{-1}, in addition to a band at 1467 cm^{-1} which may be attributed to $\delta(CH_2)$. The band at 1713 cm^{-1} is attributed to $\nu(C=O)$ originating from carboxylic acid moieties in glutamate residues. Note that at pH 7, the latter band is not observed suggesting a complete deprotonation of carboxylic acid groups (Figure 4B). The integrated intensity of amide bands and C=O stretching band was then used to provide a rough comparison of the amounts of adsorbed peptide, at pH 3 or 7. Interestingly, these band intensity increased markedly with increasing the incubation time when adsorption is performed at pH 3 (Figure 4C), i.e. where the dissolution rate of copper is comparatively high. By contrast, no noticeable evolution of the intensity was observed at pH 7 (Figure 4C). These observations confirm the role of copper dissolution in the build-up of multilayers, as schematized in Figure 5A. Such a mechanism yields the formation of a hybrid, homogeneous and thick layer made of cuprous-peptide complex which consists in two peptide molecules anchored to a cuprous ion (cuprous-thiolate complexes ($RS-Cu^I-SR$). Moreover, by considering the cuprous-thiolate edifice depicted in Figure 5C, a thickness of 50 nm, as measured by AFM (Figure 2D), corresponds to the stacking of approximately twenty $RS-Cu^I-SR$ complexes according to the perpendicular to the surface plan. At neutral pH, the growth of the peptide layer is rapidly stopped as the dissolution rate of

cuprous ions is not significant enough, leading to the formation of a monolayer-like structure (Figure 5B). This is, to our knowledge, the first evidence of metal dissolution-induced peptide multilayer growth in aqueous solutions.

In aerated aqueous solution, copper dissolution occurs via a two-step electron-transfer process, according to the Bockris-Mattson mechanism, [70] which assumes the oxidation of copper ($Cu \rightarrow Cu^{I} + e^{-}$) followed by the oxidation of Cu^{I} ($Cu^{I} \rightarrow Cu^{II} + e^{-}$). The reaction kinetics is limited by mass transport of oxygen, and in some situations, by the oxidation of Cu^{I} intermediate. [69] The presence of peptide molecules in solution leads to the formation of a cuprous-thiolate complex ($RS–Cu^{I}–SR$). The presence of the native copper oxide did not influence the process of multilayers growth in the studied conditions (pH 3). This was demonstrated by etching the copper surface in acidic medium prior to peptide adsorption (data not shown). The formation of the cuprous-thiolate complex is favored by the generation of cuprous ions, which, thus, can be considered as the driving force for multilayers growth. This is supported by three important observations. First, the growth of multilayers is enhanced with increasing the concentration of peptide (see AFM data, Figure 2D). Second, the build-up of multilayers was not observed on gold substrate at pH 3, i.e. where the peptide exhibits the same degree of protonation as for adsorption tests on copper surface (see QCM-D data, Figure 1C). Third, at neutral pH, i.e. at lower copper dissolution rate, the growth of peptide multilayers was not observed (see PM-IRRAS data, Figure 4C). However, it must be kept in mind that the pH also influences intermolecular interactions in the adsorbed phase. which obviously play a role in the so-formed peptide-copper(I) complexes. This is, indeed, supported by computational considerations. DFT study was performed on the neutral form of Glu-Cys-Gly peptide. Two stable conformations have been found: the T-shape and the Y-shape (see Figure 1A). The T-shape is energetically more stable at 0.45 eV compared to the Y-shape thanks to

intramolecular interactions. Furthermore, a DFT-based AIMD simulation were performed at 300K for both shapes during 1 ps. Results showed that both conformations were stable. To study intermolecular interaction, the T-shape dimer was studied by AIMD simulation during more than 1 ps. Results indicated that the dimer is more stable at 0.7 eV than the monomer through intermolecular interactions. It seems that electrostatic and H-bonding between –COOH group on a monomer and $–NH_2$ group on another stabilize the dimer. The peptide being more protonated at pH 3 than at pH 7, [71] the number of electrostatic interactions and H-bonding increase at pH 3 compared to pH 7. In the studied condition, at pH 3, the intermolecular hydrogen bonds stabilizing dimers could favour the formation of dimers and thus stabilize the peptide multilayers (Figure 5C). By contrast, at pH 7 the intermolecular interactions are not sufficient to stabilize dimers and thus multilayers. Thereby, the build-up of peptide multilayers is driving by both the generation of Cu^+ ions and stabilized by the intermolecular interactions.

4. Conclusion

In the present study, we presented a combination of *in situ* and *ex situ* characterization, which showed an unusual adsorption behavior of a small peptide on a copper surface. Results revealed the formation of a homogeneous and thick multilayers made of cuprous-peptide complex. The build-up of this hybrid multilayers is driving by the generation of Cu^+ ions in acidic medium. DFT calculations support that favorable intermolecular interaction, together with Cu^+ generation, is determining for the formation of the hybrid copper-peptide multilayers.

Acknowledgement

The authors thank Laeticia Lefebure (Sorbonne Université, LRS) for her strong involvement in this work. PC acknowledge financial support from CNRS (Emergence – INC).

References

[1] A. Rimola, D. Costa, M. Sodupe, J.-F. Lambert, P. Ugliengo, Silica Surface Features and Their Role in the Adsorption of Biomolecules: Computational Modeling and Experiments, Chemical Reviews, 113 (2013) 4216-4313.
[2] T.R. Walsh, M.R. Knecht, Biointerface Structural Effects on the Properties and Applications of Bioinspired Peptide-Based Nanomaterials, Chemical Reviews, 117 (2017) 12641-12704.
[3] J.D. Hartgerink, E. Beniash, S.I. Stupp, Self-Assembly and Mineralization of Peptide-Amphiphile Nanofibers, Science, 294 (2001) 1684-1688.
[4] M. Sarikaya, C. Tamerler, A.K.Y. Jen, K. Schulten, F. Baneyx, Molecular biomimetics: nanotechnology through biology, Nature Materials, 2 (2003) 577-585.
[5] C.R. So, J.L. Kulp, E.E. Oren, H. Zareie, C. Tamerler, J.S. Evans, M. Sarikaya, Molecular Recognition and Supramolecular Self-Assembly of a Genetically Engineered Gold Binding Peptide on Au{111}, ACS Nano, 3 (2009) 1525-1531.
[6] C.-L. Chen, N.L. Rosi, Peptide-Based Methods for the Preparation of Nanostructured Inorganic Materials, Angewandte Chemie International Edition, 49 (2010) 1924-1942.
[7] S. Zhang, Fabrication of novel biomaterials through molecular self-assembly, Nature Biotechnology, 21 (2003) 1171-1178.
[8] X. Bi, C.H. Heng, K.-L. Yang, A Method of Obtaining High Selectivity for Copper Ions on Triglycine Decorated Surfaces, The Journal of Physical Chemistry C, 112 (2008) 12887-12893.
[9] U.E. Wawrzyniak, P. Ciosek, M. Zaborowski, G. Liu, J.J. Gooding, Gly-Gly-His Immobilized On Monolayer Modified Back-Side Contact Miniaturized Sensors for Complexation of Copper Ions, Electroanalysis, 25 (2013) 1461-1471.
[10] B. Helms, I. van Baal, M. Merkx, E.W. Meijer, Site-Specific Protein and Peptide Immobilization on a Biosensor Surface by Pulsed Native Chemical Ligation, ChemBioChem, 8 (2007) 1790-1794.
[11] I.A. Banerjee, L. Yu, H. Matsui, Cu nanocrystal growth on peptide nanotubes by biomineralization: Size control of Cu nanocrystals by tuning peptide conformation, Proceedings of the National Academy of Sciences, 100 (2003) 14678-14682.
[12] H. Lu, M.A. Hood, S. Mauri, J.E. Baio, M. Bonn, R. Muñoz-Espí, T. Weidner, Biomimetic vaterite formation at surfaces structurally templated by oligo(glutamic acid) peptides, Chemical Communications, 51 (2015) 15902-15905.
[13] S.L. Bellis, Advantages of RGD peptides for directing cell association with biomaterials, Biomaterials, 32 (2011) 4205-4210.
[14] D. Costa, C.-M. Pradier, F. Tielens, L. Savio, Adsorption and self-assembly of bio-organic molecules at model surfaces: A route towards increased complexity, Surface Science Reports, 70 (2015) 449-553.
[15] V. Humblot, A. Vallée, A. Naitabdi, F. Tielens, C.-M. Pradier, Drastic Au(111) Surface Reconstruction upon Insulin Growth Factor Tripeptide Adsorption, Journal of the American Chemical Society, 134 (2012) 6579-6583.
[16] C. Methivier, V. Lebec, J. Landoulsi, C.M. Pradier, Probing the Binding Mechanism of Peptides on a Copper Surface: Multilayer Self-Assembly Promoted by Glutamate Residues, The Journal of Physical Chemistry C, 115 (2011) 4041-4046.
[17] V. Humblot, A. Tejeda, J. Landoulsi, A. Vallée, A. Naitabdi, A. Taleb, C.M. Pradier, Walking peptide on Au(110) surface: Origin and nature of interfacial process, Surface Science, 628 (2014) 21-29.

[18] J. Schneider, L. Colombi Ciacchi, Specific Material Recognition by Small Peptides Mediated by the Interfacial Solvent Structure, Journal of the American Chemical Society, 134 (2012) 2407-2413.
[19] D. Costa, L. Savio, C.M. Pradier, Adsorption of Amino Acids and Peptides on Metal and Oxide Surfaces in Water Environment: A Synthetic and Prospective Review, The Journal of Physical Chemistry B, 120 (2016) 7039-7052.
[20] S. Monti, A.C.T. van Duin, S.-Y. Kim, V. Barone, Exploration of the Conformational and Reactive Dynamics of Glycine and Diglycine on TiO2: Computational Investigations in the Gas Phase and in Solution, The Journal of Physical Chemistry C, 116 (2012) 5141-5150.
[21] S. Monti, M. Alderighi, C. Duce, R. Solaro, M.R. Tiné, Adsorption of Ionic Peptides on Inorganic Supports, The Journal of Physical Chemistry C, 113 (2009) 2433-2442.
[22] S. Monti, V. Carravetta, W. Zhang, J. Yang, Effects Due to Interadsorbate Interactions on the Dipeptide/TiO2 Surface Binding Mechanism Investigated by Molecular Dynamics Simulations, The Journal of Physical Chemistry C, 111 (2007) 7765-7771.
[23] W.-S. Choe, M.S.R. Sastry, C.K. Thai, H. Dai, D.T. Schwartz, F. Baneyx, Conformational Control of Inorganic Adhesion in a Designer Protein Engineered for Cuprous Oxide Binding, Langmuir, 23 (2007) 11347-11350.
[24] F. Meder, H. Hintz, Y. Koehler, M.M. Schmidt, L. Treccani, R. Dringen, K. Rezwan, Adsorption and Orientation of the Physiological Extracellular Peptide Glutathione Disulfide on Surface Functionalized Colloidal Alumina Particles, Journal of the American Chemical Society, 135 (2013) 6307-6316.
[25] J. Hirrlinger, R. Dringen, The cytosolic redox state of astrocytes: Maintenance, regulation and functional implications for metabolite trafficking, Brain Research Reviews, 63 (2010) 177-188.
[26] I. Ellison, J.P. Richie, Mechanisms of glutathione disulfide efflux from erythrocytes, Biochemical Pharmacology, 83 (2012) 164-169.
[27] J.P. Perdew, J.A. Chevary, S.H. Vosko, K.A. Jackson, M.R. Pederson, D.J. Singh, C. Fiolhais, Atoms, molecules, solids, and surfaces: Applications of the generalized gradient approximation for exchange and correlation, Physical Review B, 46 (1992) 6671-6687.
[28] J.P. Perdew, K. Burke, M. Ernzerhof, Generalized Gradient Approximation Made Simple, Physical Review Letters, 77 (1996) 3865-3868.
[29] P.E. Blöchl, O. Jepsen, O.K. Andersen, Improved tetrahedron method for Brillouin-zone integrations, Physical Review B, 49 (1994) 16223-16233.
[30] G. Kresse, D. Joubert, From ultrasoft pseudopotentials to the projector augmented-wave method, Physical Review B, 59 (1999) 1758-1775.
[31] S. Grimme, Semiempirical GGA-type density functional constructed with a long-range dispersion correction, Journal of Computational Chemistry, 27 (2006) 1787-1799.
[32] CP2K Package, , in.
[33] S. Goedecker, M. Teter, J. Hutter, Separable dual-space Gaussian pseudopotentials, Physical Review B, 54 (1996) 1703-1710.
[34] N. Aissaoui, L. Bergaoui, S. Boujday, J.-F. Lambert, C. Méthivier, J. Landoulsi, Enzyme Immobilization on Silane-Modified Surface through Short Linkers: Fate of Interfacial Phases and Impact on Catalytic Activity, Langmuir, 30 (2014) 4066-4077.
[35] F. Höök, M. Rodahl, B. Kasemo, P. Brzezinski, Structural changes in hemoglobin during adsorption to solid surfaces: Effects of pH, ionic strength, and ligand binding, Proceedings of the National Academy of Sciences, 95 (1998) 12271-12276.

[36] F. Höök, J. Vörös, M. Rodahl, R. Kurrat, P. Böni, J.J. Ramsden, M. Textor, N.D. Spencer, P. Tengvall, J. Gold, B. Kasemo, A comparative study of protein adsorption on titanium oxide surfaces using in situ ellipsometry, optical waveguide lightmode spectroscopy, and quartz crystal microbalance/dissipation, Colloids and Surfaces B: Biointerfaces, 24 (2002) 155-170.
[37] A. Osypova, C.A. Fustin, C.M. Pradier, J. Landoulsi, S. Demoustier-Champagne, Factors impacting protein adsorption on layer-by-layer assembled stimuli-responsive thin films, European Polymer Journal, 95 (2017) 195-206.
[38] M. Beauvais, T. Degabriel, N. Aissaoui, V. Dupres, E. Colaço, K. El Kirat, R.F. Domingos, D. Brouri, C.-M. Pradier, J. Spadavecchia, J. Landoulsi, Supramolecular Self-Assembly and Organization of Collagen at Solid/Liquid Interface: Effect of Spheroid- and Rod-Shaped TiO2 Nanocrystals, Advanced Materials Interfaces, 0 1900195.
[39] J. Landoulsi, S. Demoustier-Champagne, C. Dupont-Gillain, Self-assembled multilayers based on native or denatured collagen: mechanism and synthesis of size-controlled nanotubes, Soft Matter, 7 (2011) 3337-3347.
[40] M. Bieri, T. Bürgi, l-Glutathione Chemisorption on Gold and Acid/Base Induced Structural Changes: A PM-IRRAS and Time-Resolved in Situ ATR-IR Spectroscopic Study, Langmuir, 21 (2005) 1354-1363.
[41] M. Bieri, T. Bürgi, Adsorption kinetics of l-glutathione on gold and structural changes during self-assembly: an in situ ATR-IR and QCM study, Physical Chemistry Chemical Physics, 8 (2006) 513-520.
[42] A. Zhou, Q. Xie, Y. Wu, Y. Cai, L. Nie, S. Yao, Study of the Adsorption of Glutathione on a Gold Electrode by Using Electrochemical Quartz Crystal Impedance, Electrochemical Impedance Spectroscopy, and Cyclic Voltammetry, Journal of Colloid and Interface Science, 229 (2000) 12-20.
[43] K. Fujisawa, S. Imai, N. Kitajima, Y. Moro-oka, Preparation, Spectroscopic Characterization, and Molecular Structure of Copper(I) Aliphatic Thiolate Complexes, Inorganic Chemistry, 37 (1998) 168-169.
[44] L. Zhou, D. Powell, K.M. Nicholas, Tripodal Bis(imidazole) Thioether Copper(I) Complexes: Mimics of the CuM Site of Copper Hydroxylase Enzymes, Inorganic Chemistry, 46 (2007) 7789-7799.
[45] R.V. Parish, Z. Salehi, R.G. Pritchard, Five-Coordinate Sulfur in a Polymeric Copper(I) Thiolate Complex, Angewandte Chemie International Edition in English, 36 (1997) 251-253.
[46] C. Chen, Z. Weng, J.F. Hartwig, Synthesis of Copper(I) Thiolate Complexes in the Thioetherification of Aryl Halides, Organometallics, 31 (2012) 8031-8037.
[47] I.G. Dance, The structural chemistry of metal thiolate complexes, Polyhedron, 5 (1986) 1037-1104.
[48] N. Sandhyarani, T. Pradeep, An investigation of the structure and properties of layered copper thiolates, Journal of Materials Chemistry, 11 (2001) 1294-1299.
[49] V.S. Dilimon, J. Denayer, J. Delhalle, Z. Mekhalif, Electrochemical and Spectroscopic Study of the Self-Assembling Mechanism of Normal and Chelating Alkanethiols on Copper, Langmuir, 28 (2012) 6857-6865.
[50] C.A. Calderón, C. Ojeda, V.A. Macagno, P. Paredes-Olivera, E.M. Patrito, Interaction of Oxidized Copper Surfaces with Alkanethiols in Organic and Aqueous Solvents. The Mechanism of Cu2O Reduction, The Journal of Physical Chemistry C, 114 (2010) 3945-3957.

[51] O. Azzaroni, M. Cipollone, M.E. Vela, R.C. Salvarezza, Protective Properties of Dodecanethiol Layers on Copper Surfaces: The Effect of Chloride Anions in Aqueous Environments, Langmuir, 17 (2001) 1483-1487.
[52] M.M. Sung, K. Sung, C.G. Kim, S.S. Lee, Y. Kim, Self-Assembled Monolayers of Alkanethiols on Oxidized Copper Surfaces, The Journal of Physical Chemistry B, 104 (2000) 2273-2277.
[53] H. Ron, H. Cohen, S. Matlis, M. Rappaport, I. Rubinstein, Self-Assembled Monolayers on Oxidized Metals. 4. Superior n-Alkanethiol Monolayers on Copper, The Journal of Physical Chemistry B, 102 (1998) 9861-9869.
[54] P.E. Laibinis, G.M. Whitesides, D.L. Allara, Y.T. Tao, A.N. Parikh, R.G. Nuzzo, Comparison of the structures and wetting properties of self-assembled monolayers of n-alkanethiols on the coinage metal surfaces, copper, silver, and gold, Journal of the American Chemical Society, 113 (1991) 7152-7167.
[55] H. Keller, P. Simak, W. Schrepp, J. Dembowski, Surface chemistry of thiols on copper: an efficient way of producing multilayers, Thin Solid Films, 244 (1994) 799-805.
[56] P.E. Laibinis, G.M. Whitesides, Self-assembled monolayers of n-alkanethiolates on copper are barrier films that protect the metal against oxidation by air, Journal of the American Chemical Society, 114 (1992) 9022-9028.
[57] G. Fonder, F. Laffineur, J. Delhalle, Z. Mekhalif, Alkanethiol-oxidized copper interface: The critical influence of concentration, Journal of Colloid and Interface Science, 326 (2008) 333-338.
[58] S. Hosseinpour, M. Forslund, C.M. Johnson, J. Pan, C. Leygraf, Atmospheric corrosion of Cu, Zn, and Cu–Zn alloys protected by self-assembled monolayers of alkanethiols, Surface Science, 648 (2016) 170-176.
[59] D.S. Bergsman, T.-L. Liu, R.G. Closser, K.L. Nardi, N. Draeger, D.M. Hausmann, S.F. Bent, Formation and Ripening of Self-Assembled Multilayers from the Vapor-Phase Deposition of Dodecanethiol on Copper Oxide, Chemistry of Materials, 30 (2018) 5694-5703.
[60] L. Lecordier, S. Herregods, S. Armini, Vapor-deposited octadecanethiol masking layer on copper to enable area selective Hf3N4 atomic layer deposition on dielectrics studied by in situ spectroscopic ellipsometry, Journal of Vacuum Science & Technology A, 36 (2018) 031605.
[61] Y. Wang, J. Im, J.W. Soares, D.M. Steeves, J.E. Whitten, Thiol Adsorption on and Reduction of Copper Oxide Particles and Surfaces, Langmuir, 32 (2016) 3848-3857.
[62] N. Arisnabarreta, P.A. Paredes-Olivera, F.P. Cometto, E.M. Patrito, Growth of Layered Copper-Alkanethiolate Frameworks from Thin Anodic Copper Oxide Films, The Journal of Physical Chemistry C, (2019).
[63] F.S.M. Hashemi, S.F. Bent, Sequential Regeneration of Self-Assembled Monolayers for Highly Selective Atomic Layer Deposition, Advanced Materials Interfaces, 3 (2016) 1600464.
[64] F.S. Minaye Hashemi, B.R. Birchansky, S.F. Bent, Selective Deposition of Dielectrics: Limits and Advantages of Alkanethiol Blocking Agents on Metal–Dielectric Patterns, ACS Applied Materials & Interfaces, 8 (2016) 33264-33272.
[65] J.B. Matos, L.P. Pereira, S.M.L. Agostinho, O.E. Barcia, G.G.O. Cordeiro, E. D'Elia, Effect of cysteine on the anodic dissolution of copper in sulfuric acid medium, Journal of Electroanalytical Chemistry, 570 (2004) 91-94.
[66] A. Jürgensen, H. Raschke, N. Esser, R. Hergenröder, An in situ XPS study of L-cysteine co-adsorbed with water on polycrystalline copper and gold, Applied Surface Science, 435 (2018) 870-879.

[67] C. Wang, X. Luo, Z. Jia, Linkage, charge state and layer of L-Cysteine on copper surfaces, Colloids and Surfaces B: Biointerfaces, 160 (2017) 33-39.
[68] K. Uvdal, P. Bodö, B. Liedberg, l-cysteine adsorbed on gold and copper: An X-ray photoelectron spectroscopy study, Journal of Colloid and Interface Science, 149 (1992) 162-173.
[69] C.M. Galvani, A. Graydon, D.J. Riley, D. York, Electrochemical Quartz Crystal Microbalance in a Channel Flow Cell: A Study of Copper Dissolution, The Journal of Physical Chemistry C, 111 (2007) 3669-3674.
[70] E. Mattsson, J.O.M. Bockris, Galvanostatic studies of the kinetics of deposition and dissolution in the copper + copper sulphate system, Transactions of the Faraday Society, 55 (1959) 1586-1601.
[71] D. Vila-Viçosa, V.H. Teixeira, H.A.F. Santos, M. Machuqueiro, Conformational Study of GSH and GSSG Using Constant-pH Molecular Dynamics Simulations, The Journal of Physical Chemistry B, 117 (2013) 7507-7517.

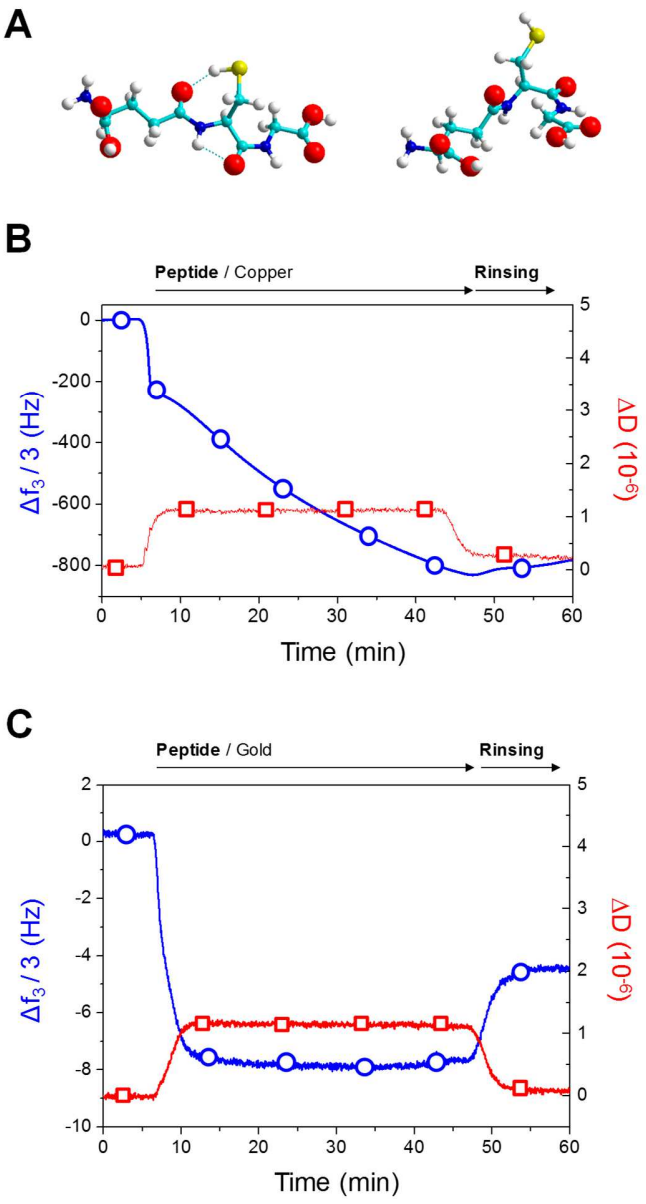

Figure 1. (A) Molecular structure of the Glu-Cys-Gly peptide used in this study: T-shape on the left and Y-shape on the right. T-shape is the most stable conformation. (B, C) *In situ* QCM-D measurements showing frequency changes in the 3rd overtone and the corresponding dissipation changes during the adsorption of the peptide on (B) copper or (C) gold surface. Arrows on top of the graphs indicate the start and duration of injection of peptide solution (10 mM), and the rinsing step with ultrapure water.

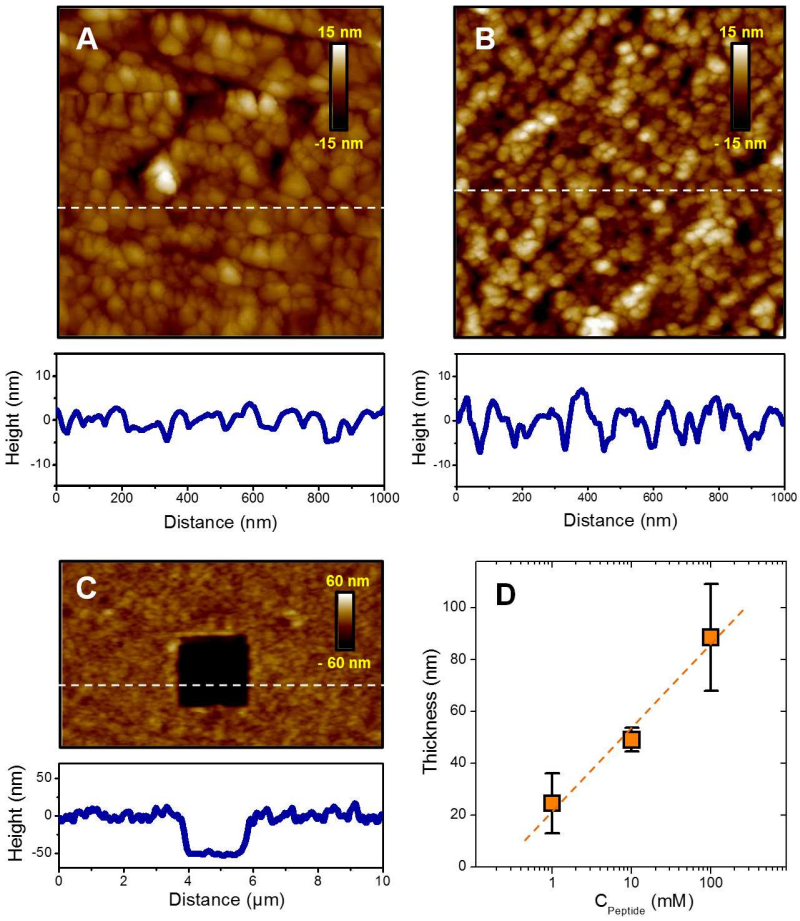

Figure 2. (A, B) AFM height images (1 µm × 1 µm, peak force tapping mode, in ultrapure water) recorded on copper substrate (A) prior to and (B) after the adsorption of the Glu-Cys-Gly peptide (10 mM) for 1 h. Cross-sections are taken at the locations indicated by dashed lines. (C) AFM image (10 µm × 10 µm, contact mode, in water) of the scratch on the peptide layer using AFM tip (top), and the profile of the line of the surface scan (bottom). (D) Evolution of the peptide layer thickness, as determined by AFM scratch tests, as a function of the concentration of peptide solution.

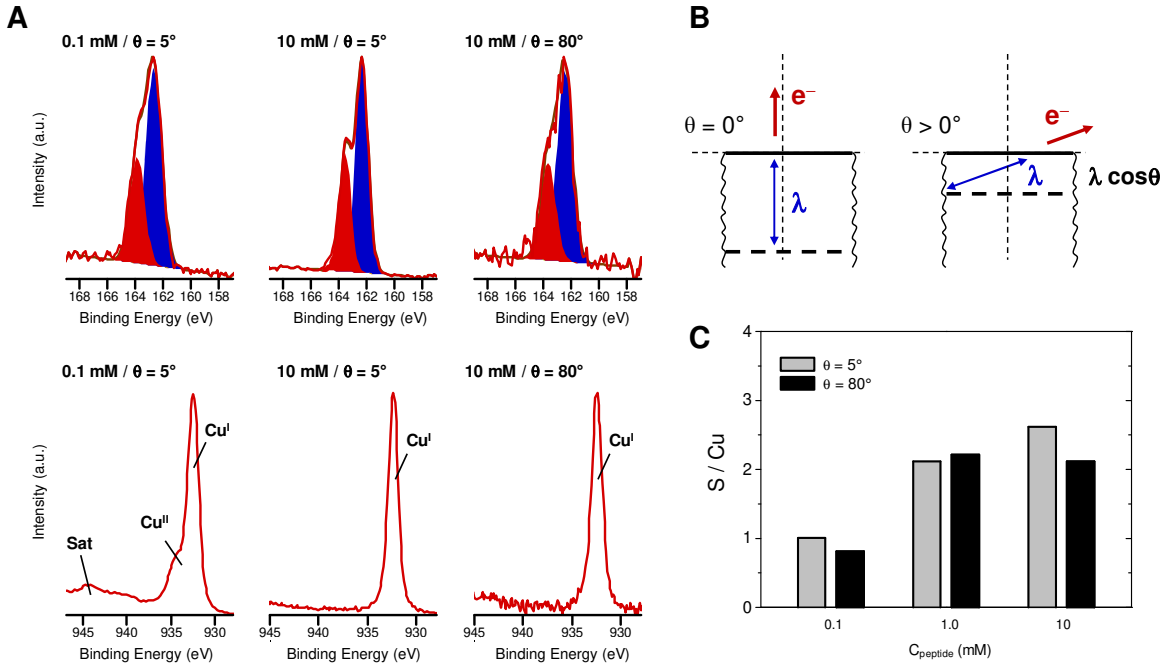

Figure 3. (A) Typical S 2p (top) and Cu $2p_{3/2}$ (bottom) peaks recorded on copper substrate after the adsorption of Glu-Cys-Gly peptide at a concentration of 0.1 or 10 mM. Spectra were recorded at take-off angle θ = 5 or 80°, as indicated. (B) Schematic representation showing the evolution of the analysis depth as a function of the take-off angle θ. (C) Histograms showing the evolution of the S/Cu molar concentration ratio as a function of the concentration of peptide solution: θ = 5° (gray) and 80° (black).

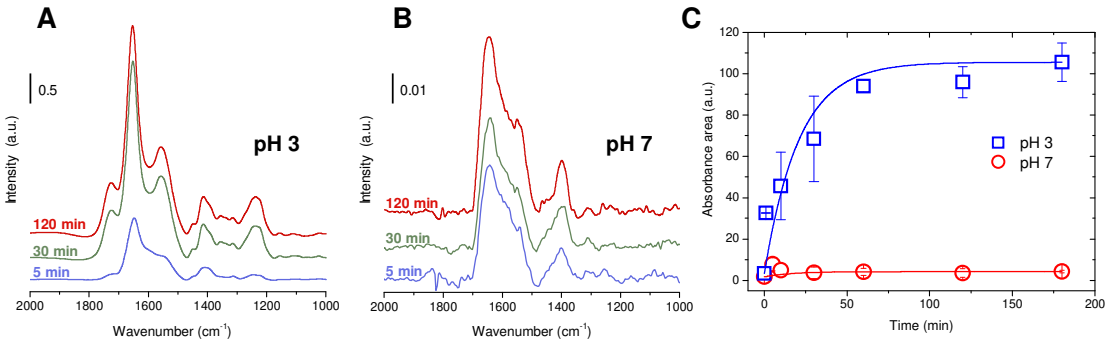

Figure 4. (A, B) PM-IRRAS spectra recorded on copper surface after incubation in peptide solutions (10 mM) at (A) pH 3 or (B) pH 7 for 5, 30 and 120 min. (C) Evolution of the integrated intensity of amide bands and C=O stretching band as a function of the incubation time (from 5 to 180 min) in peptide solutions (10 mM) at pH 3 (squares) and 7 (circles).

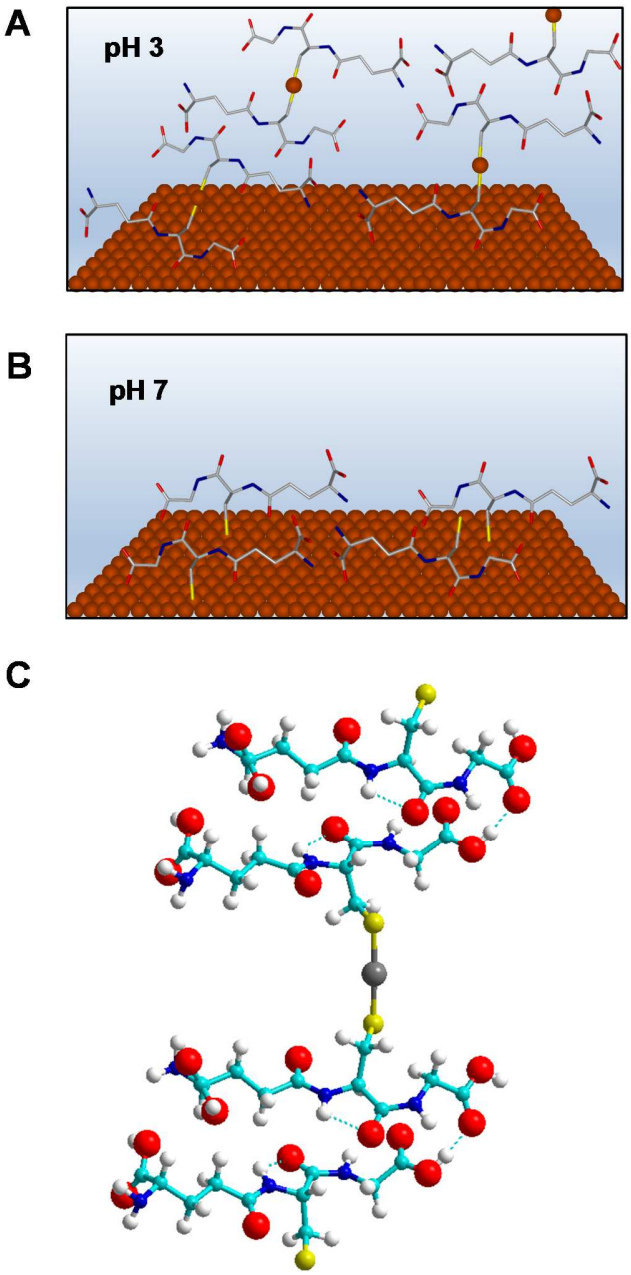

Figure 5. (A, B) Proposed mechanism of peptide multilayer growth on copper surface. (A) Growth of hybrid multilayers, at pH 3, composed of peptide and Cu^{I} species which form cuprous-thiolate complex following a 1:2 relationship. (B) Formation of a monolayer-like structure of peptides, all sulfur being bound to copper. (C) Optimized structure of two dimers bridging a copper.